The 2012 World Congress on
Advances in Civil, Environmental, and Materials Research (ACEM' 12)
Seoul, Korea, August 26-30, 2012

A coupled soil-pore fluid formulation for modeling soil liquefaction and cyclic mobility in seabed using the finite volume method

*Tian Tang[1)], Johan Roenby [2)] and Ole Hededal [3)]

[1), 3)] *Department of Civil Engineering, Technical University of Denmark, Lyngby, Denmark*
[2)] *DHI, Hoersholm, Denmark*
* *tiat@byg.dtu.dk*

ABSTRACT

The stability of offshore structures, such as wind turbine foundations, breakwaters, and immersed tunnels can be strongly affected by the liquefaction and cyclic mobility phenomena in the seabed. Our goal is to develop a numerical code for analysis of these situations. For this purpose, we start by formulating the strong interactions between soil skeleton and the pore fluid via a coupled set of partial differential equations. A single bounding surface soil model capable of simulating the accumulations of pore pressures, strains, dilatancy, and strain 'softening', is then adopted for quantifying the cyclic soil constitutive relations. To deal with the high non-linearity in the equations, the finite volume (FV) method is proposed for the numerical simulation. The corresponding discretization strategies and solution algorithms, including the conventional segregated method and the more recent block matrix solver, are discussed as well. Overall, investigations in this paper provide a methodology for developing a numerical code simulating liquefaction and cyclic mobility. In future work this will be implemented in practice with the aid of the open source CFD toolbox, OpenFOAM.

1. INTRODUCTION

Soil liquefaction and cyclic mobility are two of the most important subjects in offshore engineering when the stability of offshore foundations is to be assessed. Liquefaction typically occurs in saturated loose granular soil when subject to repeated cyclic loading (e.g. waves, currents, vibration of superstructures in a marine environment). The gradual build-up of pore pressure due to compaction of the soil skeleton eventually results in a failure state of zero effective stress. Cyclic mobility, on the other hand, is characteristic for medium-dense granular soil with stabilized pore pressure and effective stresses, but with large permanent shear strains. Both of these phenomena are results of the strong interaction of the soil skeleton with the fluid present in the pore structure (generally water). Therefore, in order to model and simulate these complex phenomena more accurately, a coupled analysis of soil and pore fluid is necessary.

[1)] PhD student
[2)] Researcher
[3)] Associate Professor

The fundamental theory describing such a coupled soil-pore fluid system was first established by Biot (1941) assuming an elastic soil skeleton and a single pore fluid phase satisfying Darcy's law. Biot's theory was later extended to cope with non-linear geomaterial behaviors by Zienkiewicz (1982), Zienkiewicz & Shiomi (1984) and Zienkiewicz et al. (1990). Three general formulations, differing in the choice of unknowns, were put forward: the *u-p-U*, *u-U*, and *u-p* formulations, where *u* symbolizes the soil skeleton displacements vector, *p* is the pore fluid pressure, and *U* is the pore fluid displacements vector. The *u-p-U* formulation containing all the three unknowns is powerful in dealing with high frequency phenomena (Oka et al. 1994). The *u-U* formulation aimed at tracking the displacements of both the soil skeleton and the fluid phase has not been widely applied due to the potential volumetric locking problem in numerical simulations (Jeremic et al. 2008). The simplistic yet capable *u-p* formulation is currently the most common description used in practice (Oka et al. 1994, Elgamal et al. 2002, Di & Sato 2004, and Taiebat et al. 2007) since it is valid for low-frequency problems in dynamic analysis and reduces the total number of degrees of freedom.

Any of the above mentioned formulations for liquefaction and cyclic mobility modeling requires a well-defined constitutive law for capturing the granular seabed behavior under cyclic loading conditions. From field measurements and cyclic loading experiments, it is evident that plastic deformations occur both under loading and under unloading-reloading processes. The resulting hysteresis loop (Fig. 1.) in each cycle indicates that the soil is unable to return all the energy put into it during loading. Hence, conventional plasticity models with isotropic hardening, though adequate for modeling monotonic loading, fail to work under cyclic conditions. During the last few decades, the limitation of classical plasticity has motivated extensive efforts towards developing appropriate cyclic plasticity models. Kinematic hardening laws have been incorporated as well as models describing realistic smooth transition from elastic to fully plastic domains. Among these models, the two most successful and widely applied cyclic plasticity concepts are the *multi-surface plasticity* proposed by Mroz (1967), and the *bounding surface plasticity* by Dafalias and Popov (1975). In the branch of multi-surface plasticity, Prevost (1985) applied a simple multi-surface J_2 theory for frictional cohesionless soils. Elgamal et al. (2002) and Elgamal et al. (2003) further updated Prevost's model and applied it to the subject of earthquake engineering. Recently, Yang & Elgamal (2008) put forward a new multi-surface model considering the Lode angle effect to capture the three-dimensional loading conditions. The bounding surface theory has also been extended by several researchers (Bardet 1986, Crouch et al. 1994, Manzari & Dafalias 1997, and Li et al. 1999) to capture more realistic soil behavior such as strain softening, state dependence, fabric anisotropy, and the behavior under multi-axial loading conditions.

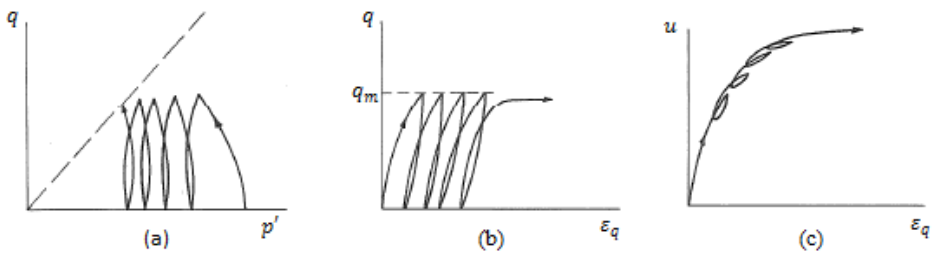

Fig. 1. Typical soil response observed during undrained cyclic loading: (a) effective stress path; (b) stress:strain response; (c) pore pressure:strain response (from Wood 1990).

Numerical simulations of hysteretic soil behavior and pore fluid pressure accumulation have mainly been conducted using the finite element method (Zienkiewicz et al. 1993, Huang & Zienkiewicz 1998, Pastor et al. 2000, and Taiebat et al. 2007), or a combination of finite element and the finite difference method (Oka et al. 1994, and Di & Sato 2003). Due to the complexity of cyclic plasticity, these coupled models are not implemented into commercial engineering software packages presently applied in engineering practice. The objective of this paper is therefore to develop a numerical code for analysis of liquefaction and cyclic mobility, which is applicable in the practical context of offshore engineering. In the following sections we will present the methodology on achieving this goal.

2. GOVERNING EQUATIONS FOR THE COUPLED SYSTEM

In this section, a mathematical framework is introduced for quantifying the behavior of the coupled soil-pore fluid system. We adopt the method of the *u-p* formulation (Zienkiewicz & Shiomi 1984, Zienkiewicz et al. 1990, Oka et al. 1994), which has the soil skeleton displacements and the pore fluid pressure as the principal unknowns. Some fundamental assumptions are made:

1) The soil grains are incompressible;
2) The soil skeleton strains remain sufficiently small;
3) The relative acceleration of the fluid phase to the solid phase is much smaller than the acceleration of the solid phase, i.e. $\dot{v}_i^f - \dot{v}_i^s \ll \dot{v}_i^s$. Where $v_i^{f(s)}, \dot{v}_i^{f(s)}$ are the velocity and acceleration of the fluid (solid) phase, respectively;

The general formulations are then derived one by one from conservation equations.

First, consider the overall momentum equation for the soil mixture:

$$(1-n)\rho_s \dot{v}_i^s + n\rho_f \dot{v}_i^f = \sigma_{ij,j} + (1-n)\rho_s b_i + n\rho_f b_i, \tag{1}$$

Here, n is the porosity; ρ_s and ρ_f are the densities of solid and fluid phase, respectively; $\sigma_{ij,j}$ stands for the divergence of the total soil stress tensor; and b_i is the body force acceleration.

Defining the mixture density $\rho = (1-n)\rho_s + n\rho_f$ and applying the third assumption above, Eq. (1) is reduced to:

$$\rho \dot{v}_i^s = \sigma_{ij,j} + \rho b_i, \tag{2}$$

Next, based on the mass balances of the solid phase and the fluid phase, and the state of equation for the fluid that reads $\dot{\rho}_f/\rho_f = \dot{p}/K_f$, the following equation can be derived:

$$\frac{n}{K_f}\dot{p} + v_{i,i}^s + n\left(v_i^f - v_i^s\right)_{,i} = 0, \tag{3}$$

Here p represents the pore fluid pressure and K_f is the bulk modulus of the pore fluid. The last term in Eq. (3) is the specific discharge. It can be rewritten using the momentum equation for the pore fluid phase,

$$n\rho_f \dot{v}_i^f = np_{,i} + n\rho_f b_i + \frac{n^2\gamma_w}{k}\left(v_i^f - v_i^s\right), \tag{4}$$

where the last term is the Darcy drag force due to friction with the skeleton with k denoting the scalar permeability coefficient and γ_w denoting the unit weight of fluid. Inserting the specific discharge from Eq. (4) in the last term of Eq. (3), and employing assumption 3) to replace $\dot{v}_i^f$ with $\dot{v}_i^s$, we obtain the equation

$$\frac{n\gamma_w}{K_f k}\dot{p} + \frac{\gamma_w}{k} v_{i,i}^s + \rho_f \dot{v}_{i,i}^s - p_{,ii} - \rho_f b_{i,i} = 0, \tag{5}$$

To further formulate the obtained governing equations - Eq. (2) and Eq. (5) in terms of our interested unknowns (u^s, p), the following relations are specified:

a) The effective stress concept: $\Delta\sigma_{ij} = \Delta\sigma'_{ij} + \alpha\delta_{ij}(\Delta p)$, where $\Delta\sigma'_{ij}$ and $\Delta\sigma_{ij}$ represent, respectively, the increment of effective stress and total stress, Δp is the incremental pore fluid pressure, δ_{ij} is the Kronecker delta and α is the Biot-Willis coefficient in the range of $n \leq \alpha \leq 1$, (Wang 2000);
b) The nonlinear stress-strain relations of soil skeleton: $\Delta\sigma'_{ij} = D_{ijkl}(\Delta\varepsilon_{kl})$. D_{ijkl} stands for the tangential stiffness matrix defined by state variables (e.g. σ', ε), the direction of the increment and/or other considerations (loading history, strain rate, etc.). Details about this matrix will be presented in section 3;
c) The linear strain-displacement relation of soil skeleton: $\Delta\varepsilon_{ij} = \frac{1}{2}\left(\Delta u_{i,j}^s + \Delta u_{j,i}^s\right)$;
d) The velocity-displacement and acceleration-displacement relations of soil skeleton: $v_i^s = \dot{u}_i^s$ and $\dot{v}_i^s = \ddot{u}_i^s$.

Based on the above specification, since it is more convenient to keep the unknowns in incremental form due to the incremental stress-strain relationship, Eq. (2) and Eq. (5) can be rewritten as:

$$-\rho\Delta\ddot{u}_i^s + \left(D_{ijkl}\Delta u_{l,k}^s\right)_{,j} + \alpha\Delta p_{,i} + \rho\Delta b_i = 0, \tag{6}$$

$$\frac{n\gamma_w}{K_f k}\Delta\dot{p} + \frac{\gamma_w}{k}\Delta\dot{u}_{i,i}^s + \rho_f\Delta\ddot{u}_{i,i}^s - \left(\Delta p_{,i}\right)_{,i} - \rho_f\Delta b_{i,i} = 0, \tag{7}$$

With the soil skeleton displacement and pore fluid pressure present simultaneously in all the governing equations, the strong interaction in the soil-pore fluid system is modeled.

3. CONSTITUTIVE MODELING

To this point, the most crucial work left is an appropriate constitutive law describing the cyclic soil stress-strain relationship, i.e. the determination of the tangential soil stiffness matrix D_{ijkl},.

The key issues in the selection of a plasticity model for the analysis of soil-fluid interaction are a) the ability to alter the void ratio of the soil, since it is this feature that allows pore pressures to develop irreversibly, leading e.g. to liquefaction; and b) a realistic but preferably numerically simple method for modeling the cyclic behavior of soil.

During the last thirty years, soil constitutive models that are able to capture the accumulations of pore pressures and strains upon cycling have been developed largely by introducing the multi-surface plasticity and the bounding surface plasticity concepts (Prevost 1985, Bardet 1986, Manzari & Dafalias 1997, Elgamal et al. 2003, and Yang & Elgamal 2008, etc.). The multi-surface plasticity is characterized by an approximation of

the actual stress-strain curve by *n* linear segments of constant stiffness moduli. The bounding surface plasticity model is featured with continuously changed stiffness moduli depending on the distance from current stress state to a correspondent image state on the prescribed bounding surface. Since both of the two cyclic plasticity theories have merits and shortcomings, a comparison is presented in Appendix I. The purpose is to select a model, which is effective enough to describe the cyclic soil behavior and yet economic enough to be implemented and applied in practice.

As a result, Bardet's single bounding surface model which has a very simple surface definition, few model constants as well as straightforward mapping technique will be chosen for the practical implementation. The numerical efficiency of Bardet's model is also considered positive since only the bounding surface must be updated in each increment, and the evolution of the surface is controlled by the volumetric strains as in classical Cam Clay models. The essential elements of this model are presented in the following.

3.1 General constitutive equations

Classically, the increment of strain resulting from a stress increment is assumed as the sum of the elastic ($\Delta\varepsilon_{ij}^{e}$) and plastic ($\Delta\varepsilon_{ij}^{p}$) incremental strains:

$$\Delta\varepsilon_{ij} = \Delta\varepsilon_{ij}^{e} + \Delta\varepsilon_{ij}^{p}, \tag{8}$$

Hence, the elastic constitutive equation can be written as:

$$\Delta\sigma_{ij}' = E_{ijkl}\,(\Delta\varepsilon_{kl}^{e}) = E_{ijkl}(\Delta\varepsilon_{kl} - \Delta\varepsilon_{kl}^{p}), \tag{9}$$

E_{ijkl} is the isotropic elastic stiffness tensor: $E_{ijkl} = K\delta_{ij}\delta_{kl} + G(\delta_{ik}\delta_{jl} + \delta_{il}\delta_{jk} - \frac{2}{3}\delta_{ij}\delta_{kl})$, in which K stands for the bulk modulus and G is the shear modulus.

The increment of plastic deformation tensor can be defined through the flow rule,

$$\Delta\varepsilon_{ij}^{p} = \langle L\rangle m_{ij}. \tag{10}$$

Here, m is a dimensionless symmetric second-order tensor indicating the 'direction' of the plastic strain determined by the outward normal to a plastic potential surface; L is the loading function, and the symbol <> denotes the McCauley's bracket so that $\langle L\rangle = L$ if $L \geq 0$; otherwise $\langle L\rangle = 0$. The loading function is defined as:

$$L = \frac{1}{H}(n_{ij}\Delta\sigma_{ij}'), \tag{11}$$

In Eq. (11), $H$is the plastic modulus, and n, which is also a symmetric second-order tensor, is the outward normal to the convex yield (bounding) surface. Substituting Eq. (9)-(10) into Eq. (11), the expression for the loading function can be re-written with respect to the strain increments:

$$L = \frac{n_{ij}E_{ijkl}}{H + n_{pq}E_{pqrs}m_{rs}}\Delta\varepsilon_{kl}, \tag{12}$$

Combing Eq. (9)-(10) and Eq. (12), it is now possible to form the full stress-strain relationship and thus obtain D_{ijkl}:

$$\Delta\sigma'_{ij} = E_{ijkl}(\Delta\varepsilon_{kl} - \langle L\rangle m_{kl}) = \left\{E_{ijkl} - \frac{E_{ijpq}m_{pq}n_{rs}E_{rskl}}{H+n_{pq}E_{pqrs}m_{rs}}\right\}\Delta\varepsilon_{kl} = D_{ijkl}(\Delta\varepsilon_{kl}), \qquad (13)$$

Most plastic models can fit within the above general framework. What makes a model unique is the specification of n, m and H, i.e. the yield (bounding) surface, the plastic potential and the plastic modulus. The specified features for Bardet's model are summarized in the following.

3.2 Bounding surface and radial mapping

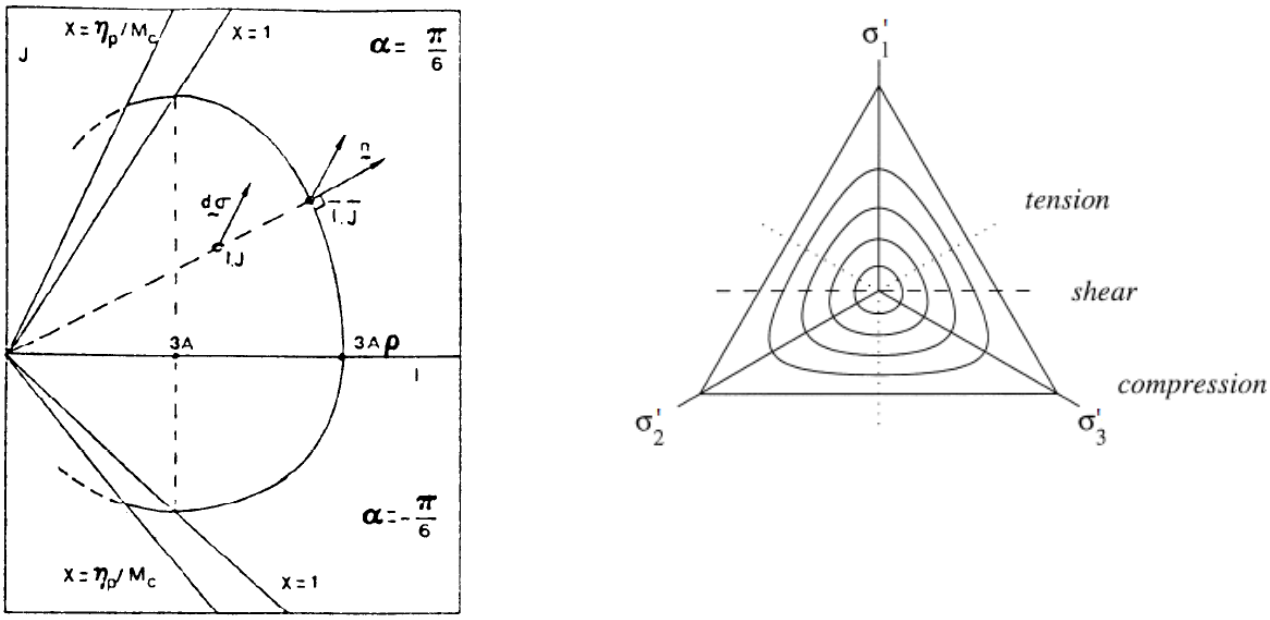

Fig. 2. left) an illustration of bounding surface, the radial mapping and image points in *I-J* space (Bardet, 1986); right) a smooth triangular contour of the surface in the deviatoric plane (Krenk 2000, LeBlanc et al. 2008).

In the model, the bounding surface is selected as a Cam-Clay type ellipse with $3A'$ as the coordinate of the ellipse summit on the I axis and ρ' as the aspect ratio in Fig. 2:

$$f(\tilde{I},\tilde{J},A) = \left(\frac{\frac{\tilde{I}}{3}-A'}{\rho'-1}\right)^2 + 3\left(\frac{\tilde{J}}{M(\theta)}\right)^2 - A'^2 = 0, \qquad (14)$$

In Eq. (14), I is the first effective stress invariant, J is the second effective deviatoric stress invariant, the tilde ($\sim$) denotes the image stress point, and θ is the Lode's angle. The definitions of the stress invariants can be found in Appendix II. The generalization of the

critical state slope *M* into the three-dimensional stress space is done by representing the deviatoric contour by a triangular shape function (Fig. 2. right):

$$M(\theta) = \frac{\cos(\gamma) M_c}{\cos\left\{\frac{1}{3}\arccos[\cos(3\gamma)\cos(3\theta)]\right\}}, \quad \gamma = \frac{\pi}{3} + \arctan\frac{1-2\frac{M_e}{M_c}}{\sqrt{3}}, \tag{15}$$

Where M_c and M_e are the critical state slope obtained from triaxial compression and extension tests, respectively.

The position of the ellipse summit is obtained similarly to the classic Cam Clay model:

$$A' = A'_0 exp\left(\frac{\Gamma - e - \kappa ln(\frac{I}{3})}{\lambda - \kappa}\right), \tag{16}$$

In above, $A'_0, \Gamma, \lambda, \kappa$ are respectively the unit pressure, critical void ratio at unit pressure, slopes of virgin loading and unloading-reloading line; and e is the current void ratio. The bounding surface may expand or shrink depending upon whether the plastic volumetric strain increases or decreases, and it must always enclose the current stress state.

The radial mapping technique generates the image stress point as the intersection of bounding surface with straight line through the origin and the current stress state. If considering an associated flow rule, it is then possible to obtain the following relationships:

$$m_{ij} = n_{ij} = \tilde{n}_{ij} = \frac{\frac{\partial f}{\partial \tilde{\sigma}'_{ij}}}{\sqrt{\frac{\partial f}{\partial \tilde{\sigma}'_{kl}} \frac{\partial f}{\partial \tilde{\sigma}'_{kl}}}}, \tag{17}$$

Notice that other considerations such as non-associated plastic potential are also possible.

3.3 Plastic modulus

The most important feature of this bounding surface model is an analytically prescribed function about the dependence of the plastic modulus H on H_b (the bounding surface plastic modulus):

$$H = H_b + S(\eta_p, \eta, M(\theta), I)\frac{\delta}{\delta_{max} - \delta}, \tag{18}$$

so that $H = +\infty$ when the distance between stress point and image point is larger than a reference distance δ_{max}, representing a purely elastic behavior; while $H = H_b$ when the two points coincide. The distance parameter δ is calculated from $\delta = \left|\tilde{\sigma}'_{ij} - \sigma'_{ij}\right|$ and the function S is an experimentally determined positive function depending on the mean stress and peak stress so as to simulate the strain-softening (Bardet 1986).

To determine the bounding surface plastic modulus H_b, two conditions are considered. Firstly, the consistency condition at the image points implies that:

$$df(\tilde{\sigma}', A') = \frac{\partial f}{\partial \tilde{\sigma}'_{ij}} d\tilde{\sigma}'_{ij} + \frac{\partial f}{\partial A'} dA' = 0, \tag{19}$$

Secondly, the stress increments at stress point and at image point on the bounding surface gives the same plastic strain increment, which leads to the expression:

$$\Delta\varepsilon_{ij}^{p} = \langle \frac{1}{H}(n_{kl}\Delta\sigma'_{kl})\rangle\, n_{ij} = \langle \frac{1}{H_b}(n_{kl}\Delta\tilde{\sigma}'_{kl})\rangle\, n_{ij}, \tag{20}$$

Recalling the volumetric hardening law for the surface evolution, and after some simple mathematical manipulations on Eq. (16), (17), (19) and (20), the following expression is obtained:

$$H_b = -\frac{vA'}{\lambda - k}\frac{\partial f}{\partial A'}\frac{1}{\frac{\partial f}{\partial \tilde{\sigma}'_{kl}}\frac{\partial f}{\partial \tilde{\sigma}'_{kl}}}\frac{\partial f}{\partial \tilde{\sigma}'_{ii}}, \tag{21}$$

In above, $v = 1 + e = 1/(1-n)$ is the current specific volume.

Up to now, the constitutive equations for the cyclic stress-strain relationships have been completed.

4. FV DISCRETIZATION & SOLUTION ALGORITHM

To obtain a numerical solution, an appropriate discretisation strategy is necessary. Conventionally, solid body problems have been tackled mainly by the finite element method (FEM); however, for this cyclic soil behavior analysis, the presence of the non-linear term – the tangential matrix D_{ijkl} complicates the system significantly that using FEM can be quite expensive. Alternatively, the present paper is attempting to apply the finite volume method (FVM) for the simulation, which is motivated by the appealing capacity of FVM in solving highly non-linear problems in computational fluid dynamics.

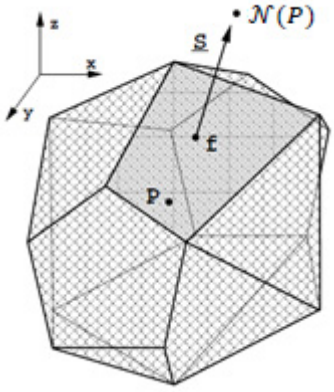

Fig. 3. Control volume: *P* is the centroid, *f* for the face centre, *S* for the face area vector, and $\mathcal{N}(P)$ for an assemblage of centroids in neighboring CVs (from Jasak & Weller) 2000).

Discretization of the computational domain consists of both temporal and spatial discretization: the time is discretized into an arbitrary number of time steps (δt), and the problem domain is subdivided into a finite number (*N*) of contiguous control volumes (CV), where the computational points lie in the centre (see illustration in Fig. 3 above).

The Eq. (6)-(7) can now be integrated over each of the N CV's giving the 4N equations

$$\int_{V_P} \underbrace{\left(D_{ijkl}\Delta u^s_{l,k}\right)_{,j}}_{S1^*} dV + \int_{V_P} \underbrace{\left(\alpha \Delta p_{,i}\right)}_{S2} dV - \int_{V_P} \underbrace{\left(\rho \Delta \ddot{u}^s_i\right)}_{T1+S3} dV + \int_{V_P} (\rho \Delta b_i) dV = 0, \quad (22)$$

$$\int_{V_P} \underbrace{\left(\frac{n\gamma_w}{K_f k}\Delta \dot{p}\right)}_{T2+S3} dV + \int_{V_P} \underbrace{\left(\frac{\gamma_w}{k}\Delta \dot{u}^s_{i,i}\right)}_{T2+S2} dV - \int_{V_P} \underbrace{\left(\left(\Delta p_{,i}\right)_{,i}\right)}_{S1} dV + \int_{V_P} \underbrace{\left(\rho_f \Delta \ddot{u}^s_{i,i}\right)}_{T1+S2} dV - \int_{V_P} (\rho_f \Delta b_{i,i}) dV = 0, \quad (23)$$

The approximations of different derivative terms in above can be attained generally by applying Gauss theorem and some single time step schemes (Newmark 1959, Krenk 1999) summarized in Table 1:

Table. 1. Generalized approximation scheme

Spatial approximation	S1*	$\int_{V_P}\left(D_{ijkl}\Delta u^s_{l,k}\right)_{,j} dV = \oint_{S_P}\left(D_{ijkl}\Delta u^s_{l,k}\right) dS_j \cong \sum_f \left(D_{ijkl}\Delta u^s_{l,k}\right)^f S_j$	The nonlinear term $\left(D_{ijkl}\right)^f$ needs special attention.
	S1	$\int_{V_P}\left(\vartheta\left(\Delta\phi_{,i}\right)_{,i}\right) dV = \oint_{S_P}\left(\vartheta\Delta\phi_{,i}\right) dS_i \cong \sum_f \vartheta^f\left(\Delta\phi_{,i}\right)^f S_i^f$	$\Delta\phi$ = general variables $(\Delta u_i, \Delta p)$, ϑ = corresponding general coefficients, S_i =surface area vector f = face β_1, β_2 = scheme parameters in range: $\beta_1 \geq 1/2$ $\beta_2 \geq 1/2$ $\dot{\phi}^o, \ddot{\phi}^o$=old-time values.
	S2	$\int_{V_P}\left(\vartheta\Delta\phi_{,i}\right) dV = \oint_{S_P}\left(\vartheta\Delta\phi\right) dS_i \cong \sum_f \vartheta^f\left(\Delta\phi\right)^f S_i^f$	
	S3	$\int_{V_P}\left(\vartheta\Delta\phi\right) dV \cong \vartheta_P \Delta\phi_P V_P$	
Temporal approximation	T1	$\Delta\ddot{\phi} \cong \frac{\Delta\phi - \delta t\dot{\phi}^o - \frac{1}{2}(\delta t)^2\ddot{\phi}^o}{\beta_1(\delta t)^2}$	
	T2	$\Delta\dot{\phi} \cong \frac{\Delta\phi - \delta t\dot{\phi}^o}{\beta_2(\delta t)}$	

With an assumption of a linear variation of the variables over the CV, there are several existing approaches for approximating the increments of face gradient $\left(\Delta\phi_{,i}\right)^f$ and face value $(\Delta\phi)^f$ from the computing centroids $(\Delta\phi^P)$ and neighboring centroids $(\Delta\phi^{\mathcal{N}(P)\cdot})$, available in the literature (Jasak & Weller 2000, Demirdzic & Martinovic 1993, Demirdzic & Muzaferija 1995). The biggest challenge for our problem lies in how to treat the nonlinear term D_{ijkl}, since it depends on the current stresses, hardening parameter, and displacements as well. It has been demonstrated that explicit treatment of D_{ijkl} tends to overestimate the stiffness and results in cumulative errors (Krenk 1993). Therefore, a convergent iterative process using Newton's procedure is necessary to correct the solutions in each time step.

At present, to discuss the solution algorithm alone, the assembled discretisation equations for the P_{th} control volume are written:

$$a_{ij}^{PP}\Delta u_j^P + \sum_{Q\in\mathcal{N}(P)} a_{ij}^{PQ}\Delta u_j^Q + \underbrace{b_i^{PP}\Delta p^P + \sum_{Q\in\mathcal{N}(P)} b_i^{PQ}\Delta p^Q}_{pressure-displacement\ coupling} = c_i^P \tag{24}$$

$$d^{PP}\Delta p^P + \sum_{Q\in\mathcal{N}(P)} d^{PQ}\Delta p^Q + \underbrace{e_j^{PP}\Delta u_j^P + \sum_{Q\in\mathcal{N}(P)} e_j^{PQ}\Delta u_j^Q}_{displacement-pressure\ coupling} = f^P \tag{25}$$

Here a, b, d, e represent, respectively, the different forms of the discretized coefficients from Eq. 22 and 23; c, f stand for the source terms including the body force, old time values and boundary conditions; the superscript Q is another index like P to address the influences between cells, and the set of neighbor cells to P is denoted by $\mathcal{N}(P)$.

Conventionally, such an algebraic system is solved by applying the segregated method. This is an iterative solution scheme where one considers the first equation as an equation for the first component Δu_1, the second and third equations as equations for Δu_2 and Δu_3, respectively and the final equation as an equation for p. It treats the inter-component displacement coupling and the pressure coupling in Eq. (24) explicitly from guessed or previously iterated values, shifting them into source terms so as to solve each component of displacement increments successively. Afterwards, explicit displacement coupling is applied to attain the pressure increment in Eq. (25). The solution algorithm is illustrated in the figure below:

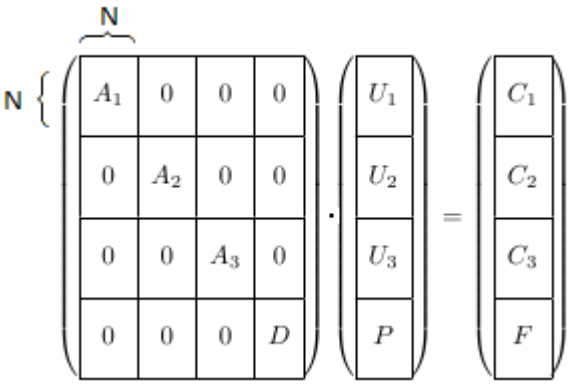

Fig. 4. Segregated method, a variable-based sorted algorithm

Where,

$A_i = N \times N$ sparse matrix with a_{ii}^{PP} on the diagonal and a_{ii}^{PQ} on the off-diagonals;
$D = N \times N$ sparse matrix with d^{PP} on the diagonal, and d^{PQ} on the off-diagonals;
$U_i = [\Delta u_i^1, \Delta u_i^2, \cdots, \Delta u_i^N]^T$; $P = [\Delta p^1, \Delta p^2, \cdots, \Delta p^N]^T$;
$C_1 = c_1 + c_1^*(\Delta u_2^*, \Delta u_3^*, \Delta p^*)$, $C_2 = c_2 + c_2^*(\Delta u_1^*, \Delta u_3^*, \Delta p^*)$, $C_3 = c_3 + c_3^*(\Delta u_1^*, \Delta u_2^*, \Delta p^*)$;
$F = f + f^*(\Delta u_1^*, \Delta u_2^*, \Delta u_3^*)$.

It is noted that the number of off-diagonal non-zero elements in the P_{th} row of A_i and D equals the number of neighbors of the P_{th} cell. The asterisk notation represents the additional source terms created from explicit treatment of couplings.

The segregated method is solving one variable for the whole domain once and then moves on to the next variables consecutively. A few iterations are needed to correct the solutions in each discretized time step. The method is economic since the large system has been split into four sub-systems for each variable and the sub-system is diagonally dominant, and thus well-suited for iterative solvers. However, the limitation of this method lies in that it can only be expected to converge for weakly coupled problems. For our strongly coupled system, this explicit treatment of coupling could cause very slow (or even no) convergence. Thus a fully implicit algorithm being able to solve all the displacement components and the pore pressures simultaneously would be more suitable. The newly developed block matrix solver (Clifford & Jasak, 2009, Kissling et al. 2010) is providing this kind of choice by treating all the coupling terms implicitly, see illustration in below:

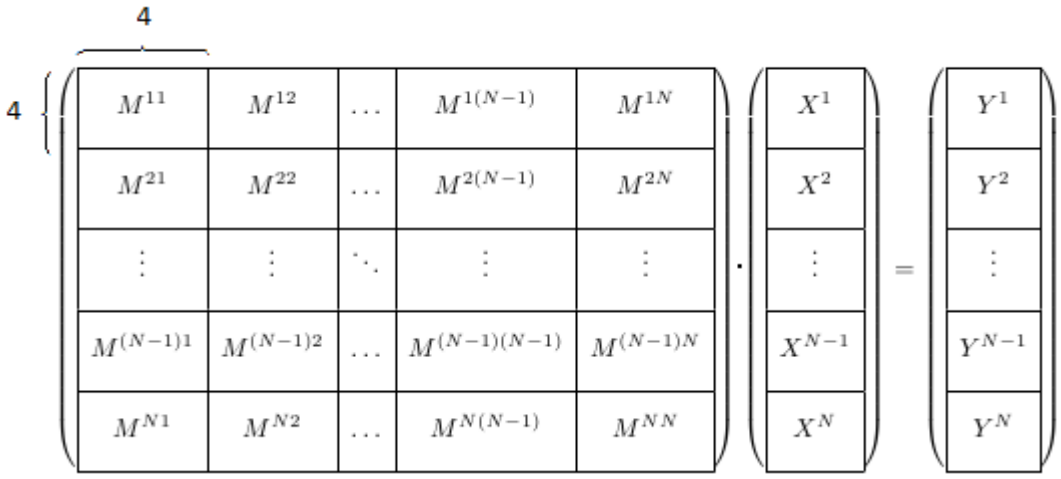

Fig. 5. Block matrix solver, a control volume-based sorted algorithm

In Fig. 5, the matrix consists of N^2 blocks of 4×4 local matrix (M), whose definition is:

$$M^{PQ} = \begin{bmatrix} a_{11}^{PQ} & a_{12}^{PQ} & a_{13}^{PQ} & b_1^{PQ} \\ a_{21}^{PQ} & a_{22}^{PQ} & a_{23}^{PQ} & b_2^{PQ} \\ a_{31}^{PQ} & a_{32}^{PQ} & a_{33}^{PQ} & b_3^{PQ} \\ e_1^{PQ} & e_2^{PQ} & e_3^{PQ} & d^{PQ} \end{bmatrix}$$

All the unknown variables are arranged cell by cell, with the same strategy for the source terms, shown below:

$$X^P = \begin{bmatrix} \Delta u_1^P \\ \Delta u_2^P \\ \Delta u_3^P \\ \Delta p^P \end{bmatrix}, \qquad Y^P = \begin{bmatrix} c_1^P \\ c_2^P \\ c_3^P \\ f^P \end{bmatrix}$$

Note that when the cell Q is not the neighbor of P, M^{PQ} is simply a zero matrix. Thus, the sparseness pattern of the matrix in Fig. 5 is the same as for A_i and D in the segregated

method shown in Fig.4, with nonzero entries only where the index pair corresponds to neighbor cells. However, this block matrix system is non-symmetrical and has much more non-zero entries compared to the system of segregated method, which would then require more computational efforts.

In general, whether to choose the segregated method or the block matrix solver method is a question of trade-off between solving a reduced cheaper system repeatedly with slow convergence, and solving a much larger system with all the coupling relations preserved.

CONCLUSION

This paper proposes the fundamental formulations and methodology of developing a numerical code modeling the soil liquefaction and cyclic mobility phenomena in the marine environment. The strong interactions between soil skeleton displacements and the pore pressure variations are mathematically modeled by a set of coupled partial differential equations. A constitutive model that appropriately describes the cyclic soil stress-strain relationships is crucial for achieving the accuracy of a numerical solution. A bounding surface model has been selected and presented in detail. In order to obtain reliable numerical simulations, the finite volume method is proposed for the discretization strategy. Different solution algorithms are discussed for solving the resulted algebraic system. Generally, it is expected that this coupled soil-pore fluid formulation incorporating the strong interactions in the porous seabed can gain more accuracy in modeling soil liquefaction and cyclic mobility compared with conventionally uncoupled approaches.

APPENDIX I. Comparisons on three constitutive models for cyclic plasticity

	Multi-surface plasticity models (*Prevost 1985, Elgamal et al. 2003, Yang & Elgamal 2008*)	**Bounding surface plasticity models**	
		The critical state two-surface model (*Manzari & Dafalias 1997*)	**The single bounding surface model** (*Bardet 1986*)
Storage requirement	A field of nested yield surfaces(location, size, plastic modulus)	Yield surface + critical surface+ bounding surface+ dilatancy surface (prescribed surface evolutions)	Bounding surface (contraction/expansion)
Model constants (with unclear physical meanings)	None (optional constants to achieve more accurate dilatancy if required)	Surface quantities: k^b & k^d Kinematic hardening constant: h_0 Dilatancy constant: A	Ellipse aspect ratio (dilatancy): ρ Plastic modulus constant: h_0
Mapping rule	None	Radial mapping	
		Three image back-stress ratio points on the dilatancy, critical, and bounding surface.	A single image stress point on the bounding surface
Adequacy in modeling smoothly varied stiffness upon loading and the dramatic changes in stiffness under shear reversal	-Segments of linear stress-strain behavior; Only if the more segments are divided, smooth transitions from elastic to plastic domain can be approximated. - Stiff (elastic) behavior immediately after shear reversal, followed by decreasing stiffness in further unloading.	-Prescribed smooth variation of the stiffness upon loading by measuring the distance from current stress state to the bounding surface. - Discontinuously shifted 'image' points under shear reversal.	
Accuracy in estimating dilatancy (*D*)	$D = 0$ only with $\eta = \eta_{PT}$ $D > 0$ at $\eta < \eta_{PT}$ or $\dot{\eta} < 0$ $D < 0$ at $\eta > \eta_{PT}$ Independent on material state	$D = 0$ with $\eta = \eta_{PT}$ or $\eta = M_{c(e)}$ The sign of *D* depends directly on whether stress point within or without the dilatancy surface	$D = 0$ with $\eta = \eta_{PT} = M_{c(e)}$ Strong dilatancy defined by small aspect ratio ρ.
Capability in simulating strain softening	Without apparent softening	Softening after peak stress ratio	Bounding surface contracts after dilation, while softening of the loading occurs after the peak stress ratio.
Potential for model extension (simulating the history-dependent soils, e.g. clay)	unclear	Incorporating an extra history surface so that plastic modulus: $K_p \propto \{d_1$(current stress point → image point on history surface) + d_2(image point on history surface → image point on bounding surface).$\}$	

APPENDIX II.

The definitions of stress invariant$s$:

$$I = \sigma'_{kk} \tag{A.1a}$$

$$J = \left(\frac{1}{2} s_{ij} s_{ij}\right)^{1/2} \tag{A.1b}$$

Where, the deviatoric stress s_{ij} is calculated by:

$$s_{ij} = \sigma'_{ij} - \frac{1}{3}\sigma'_{kk}\delta_{ij} \tag{A.2}$$

The definition of Lode's angle:

$$\theta = \frac{1}{3} sin^{-1}\left(\frac{3\sqrt{3}}{2}\frac{S^3}{J^3}\right) \tag{A.3}$$

In which, the third deviator stress invariant:

$$S = \left(\frac{1}{3} s_{ij} s_{jk} s_{ki}\right)^{1/3} \tag{A.4}$$

The stress invariants at image point based on radial mapping:

$$\tilde{I} = 3\gamma^* A' \tag{A.5a}$$

$$\tilde{J} = 3\gamma^* \eta^* A' \tag{A.5b}$$

Where η^* is the generalized stress ratio:

$$\eta^* = \frac{3\sqrt{3}J}{I} \tag{A.6}$$

The scalar γ^* can be calculated by substituting Eq.A5 and A6 into Eq.27:

$$\gamma^* = \frac{M(\theta)^2 I^2 + M(\theta) I(\rho' - 1)\sqrt{M(\theta)^2 I^2 + \rho'(\rho' - 2)J^2}}{M(\theta)^2 I^2 + 27(\rho' - 1)^2 J^2} \tag{A.7}$$

REFERENCE

Bardet, J.P., (1986). “Bounding surface plasticity model for sands”, *J. Eng. Mech*, Vol.**112**(11), November.

Biot, M.A., (1941). “General theory of three dimensional consolidation”*, J. appl. Phys*, Vol.**12**, 155-164.

Clifford,. I., Jasak, H., (2009). “The application of a multi-physics toolkit to spatial reactor dynamics”, *Proceedings of International Conference on Mathematics, Computational Methods & Reactor Physics (M&C 2009)*, New York.

Crouch, R.S., Wolf J.P., Dafalias Y.F., (1994). “Unified critical-state bounding surface plasticity model for soil”*, J. Eng. Mech*, Vol.**120**(11), 2251-2270.

Dafalias, Y.F., and Popov, E.P., (1975). “A model of nonlinearly hardening materials for complex loading”, *Acta. Mech.,* Vol.**21**, 173-192.

Demirdzic, I., and Martinovic, D., (1993). “Finite volume method for thermo-elasto-plastic stress analysis”, *Comput. Methods Appl. Mech. Engrg.,* **109**, 331-349.

Demirdzic, I., and Muzaferija, S., (1995). “Numerical method for coupled fluid flow, heat transfer and stress analysis using unstructured moving meshes with cells of arbitrary topology”, *Comput. Methods Appl. Mech. Engrg.,* **125**, 235-255.

Di, Y., and Sato, T., (2004). “A practical numerical method for large strain liquefaction analysis of saturated soils”, *Soil Dynamics and Earthquake Engineering*, **24**, 251-260.

Elgamal, A., Yang, Z.H., Parra, E., (2002). “Computational modeling of cyclic mobility and post-liquefaction site response”, *Soil Dynamics and Earthquake Engineering*, **22**, 259-271.

Elgamal, A., Yang, Z.H., Parra, E., and Ragheb, A., (2003). “Modeling of cyclic mobility in saturated cohesionless soils”, *Int. J. Plasticity*., **19**, 883-905.

Huang, M.S., and Zienkiewicz, O.C., (1998). “New unconditionally stable staggered solution procedures for coupled soil-pore fluid dynamic problems”, *Int. J. Numer. Engng*. **43**, 1029-1052.

Jasak, H., and Weller, H.G., (2000). “Application of the finite volume method and unstructured meshes to linear elasticity”, *Int. J. Numer. Engng.*, **48**, 267-287.

Jeremic, B., Cheng, Z., Taiebat, M., and Dafalias, Y.F., (2008). “Numerical simulation of fully saturated porous materials”, *Int. J. Numer. Anal. Mech. Geomech*., **32**, 1635-1660.

Kissling, K., Springer, J., Jasak, H., Schutz, S., Urban, K., and Piesche, M., (2010). “A coupled pressure based solution algorithm based on the volume-of-fluid approach for two or more immiscible fluids”, *V European Conference on Computational Fluid Dynamics*, Lisbon.

Krenk, S., (1993). “Non-linear analysis with finite elements”, Alborg University, Denmark.

Krenk, S., (1999). “Dynamic analysis of structures – numerical time integration”, *Course on Non-Linear Analysis of Frame Structures,* RAMBØLL, Denmark.

Li, X.S., Dafalias, Y.F., and Wang, Z.L., (1999). “State-dependent dilatancy in critical-state constitutive modeling of sand”, *Can. Geotech. J.*, **36**, 599-611.

LeBlanc, C., Hededal, O., Ibsen L.B., (2008). “A modified critical state two-surface plasticity model for sand – theory and implementation strategy”*, DCE Technical Memorandum No.8.*

Manzari, M.T., and Dafalias, Y.F., (1997). “A critical state two-surface plasticity model for sands”, *Geotechnique* 47, No. 2, 255-272.

Mroz, Z., (1967). “On the description of anisotropic hardening”, *J. Mech. Phys. Solids*., Vol. **15**, 163-175.

Newmark, N.M., (1959). “A method of computation for structural dynamics”, *Proc. Am. Soc. Civ. Engrs*, **8**, 67-94.
Oka, F., Yashima, A., Shibata, T., Kato, M., and Uzuoka, R., (1994). “FEM-FDM coupled liquefaction analysis of a porous soil using an elasto-plastic model”, *App. Sci. Research*, 52, 209-245.
Pastor, M., Li, T., Liu, X., Zienkiewicz, O.C., and Quecedo, M., (2000). “A fractional step algorithm allowing equal order of interpolation for coupled analsis of saturated soil problems”, *Mech. Cohes.-Frict. Mater.*, **5**, 511-534.
Prevost, J.H., (1985). “A simple plasticity theory for frictional cohesionless soils”, *Soil Dynamics and Earthquake Engineering*, Vol.**4**, No.1.
Taiebat, M., Shahir, h., and Pak, A., (2007). “Study of pore pressure variation during liquefaction using two constitutive models for sand”, *Soil Dynamics and Earthquake Engineering*, **27**, 60-72.
Wang, H.F., (2000). “Theory of Linear Poroelasticity – with Applications to Geomechanics and Hydrogelogy”*, Princeton University Press*.
Wood, D.M., (1990). “Soil behavior and critical state soil mechanics”*, Cambridge University Press*.
Yang, Z.H., and Elgamal, A., (2008). “Muiti-surface cyclic plasticity sand model with Lode angle effect”, *Geotech. Geol. Eng*., **26**, 335-348.
Zienkiewicz, O.C., (1982). “Basic formulation of static and dynamic behavior of soil and other porous material”, *Appl. Math. Mech*, Vol.**3**, No.4, Aug.
Zienkiewicz, O.C., Chan, A.H.C., Pastor, M., Paul, D.K., and Shiomi, T., (1990). “Static and dynamic behavior of soils: a rational approach to quantitative solutions. I. Fully saturated problems”*, Proc. R. Soc. Lond.*, A **429**, 285-309.
Zienkiewicz, O.C., Huang, M.S., Wu, J., and Wu, S.M., (1993). “A new algorithm for the coupled soil-pore fluid problem”, *Shock and Vibration*, Vol.**1**, No.1, 3-14.
Zienkiewicz, O.C., and Shiomi, T., (1984). “Dynamic behavior of saturated porous media; The generalized Biot formulation and its numerical solution”, *Int. J. Numer. Anal. Methods Geomech.,* Vol.**8,** 71-96.